Physics of the Earth and Planetary Interiors 169 (2008) 28–40

Contents lists available at ScienceDirect

Physics of the Earth and Planetary Interiors

journal homepage: www.elsevier.com/locate/pepi

Multiple Brunhes Chron excursions recorded in the West Eifel (Germany) volcanics: Support for long-held mantle control over the non-axial dipole field

Brad S. Singer[a,*], Kenneth A. Hoffman[b,a], Elisabeth Schnepp[c], Hervé Guillou[d]

[a] *Department of Geology & Geophysics, University of Wisconsin-Madison, 1215 West Dayton Street, Madison, WI 53706, USA*
[b] *Department of Physics, CalPoly-San Luis Obispo, CA, USA*
[c] *Paleomagnetic Laboratory Gams, University of Leoben, Austria*
[d] *LSCE/IPSL, Laboratoire CEA-CNRS, Gif-sur-Yvette, France*

ARTICLE INFO

Article history:
Received 17 October 2007
Received in revised form 23 April 2008
Accepted 7 May 2008

Keywords:
Argon
Geochronology
Lava
Paleomagnetism
Excursion
Non-dipole field

ABSTRACT

Volcanic records of excursional geomagnetic field behavior, in particular paleointensity estimates, are fragmentary for the Pleistocene. The West Eifel volcanic field is unique in that 12 of 66 measured lava flow sites record Virtual Geomagnetic Poles (VGPs) clustered between 34–45°N latitude and 30–50°E longitude over the Middle East and Southeast Asia. Paleointensity determinations reveal that 13 of 37 lavas erupted during times when the ambient field was weak. Specifically, results on nine transitionally magnetized and four normally magnetized lavas indicate paleofield intensities less than 30 μT associated with virtual dipole moments (VDMs) $<4 \times 10^{22}$ Am^2 [Schnepp, E., Hradetzky, H., 1994. Combined paleointensity and ^{40}Ar/^{39}Ar age spectrum data from volcanic rocks of the West Eifel field (Germany): evidence for an early Brunhes geomagnetic excursion. J. Geophys. Res 99, 9061–9076]. Until now, the age of these lava flows has been known only from imprecise ^{40}Ar/^{39}Ar dating that implied acquisition of magnetic remanence between about 570 and 450 ka. Thus, they have been interpreted to record a single, but poorly defined, excursion in the lower Brunhes Chron. To incorporate these paleofield data into the global high-resolution Geomagnetic Instability Time Scale (GITS), we have determined precise ages of groundmass from 12 excursional and 7 normally magnetized lava flows using the ^{40}Ar/^{39}Ar incremental heating method. Unspiked K–Ar age determinations from two excursional samples are indistinguishable from their ^{40}Ar/^{39}Ar results. Ages of the excursional lava flows fall into five groups at 722 ± 38, 626 ± 24, 578 ± 8, 555 ± 4, and 528 ± 16 ka (±2σ analytical uncertainties, relative to 1.194 Ma Alder Creek sanidine). The group of three excursional flows with an age of 578 ± 8 ka correspond temporally with lava flow sequences on Tahiti and La Palma that record the Big Lost excursion at 579 ± 6 ka. Eight other excursional lavas erupted from 722 to 528 ka correlate with less well-defined excursions or paleointensity minima differentially expressed in marine sediment records. Our findings that at least four, and perhaps five, temporally distinct excursions are recorded between 722 and 528 ka further suggest that each weakening of the dynamo during this period was associated with demise of the axial dipole. The VGPs produced during these excursions are found to be dispersed longitudinally across Eurasia and are remarkably similar to those associated with the calculated *south* VGPs at West Eifel for the non-axial dipole (NAD) field during the 20th century. A simple model in which the axial dipole repeatedly collapses leaving behind a residual NAD field that is largely held by stationary sources, probably in the lowermost mantle, provides an explanation for the recurrent excursional behavior during this ~200 kyr period.

1. Introduction

Excursions are defined by shifts of the geomagnetic field during otherwise stable polarity chrons that are manifested as a reduction in field intensity and Virtual Geomagnetic Poles (VGPs) which for brief, ca. 1–10 kyr, periods differ from the Geocentric Axial Dipole (GAD) and lie outside the range of expected secular variation (Laj and Channell, 2007). Despite skepticism about the veracity of excursions and their use as stratigraphic markers (Merrill and McFadden, 2005), improved sampling of marine sediments deposited at high rates and precise geochronology applied to both sediments (astrochronology) and lava flows (^{40}Ar/^{39}Ar dating) has led to broad acceptance that many globally expressed excursions punctuate the Brunhes and Matuyama polarity chrons,

* Corresponding author. Tel.: +1 608 265 8650.
E-mail address: bsinger@geology.wisc.edu (B.S. Singer).

0031-9201/$ – see front matter © 2008 Elsevier B.V. All rights reserved.
doi:10.1016/j.pepi.2008.05.001

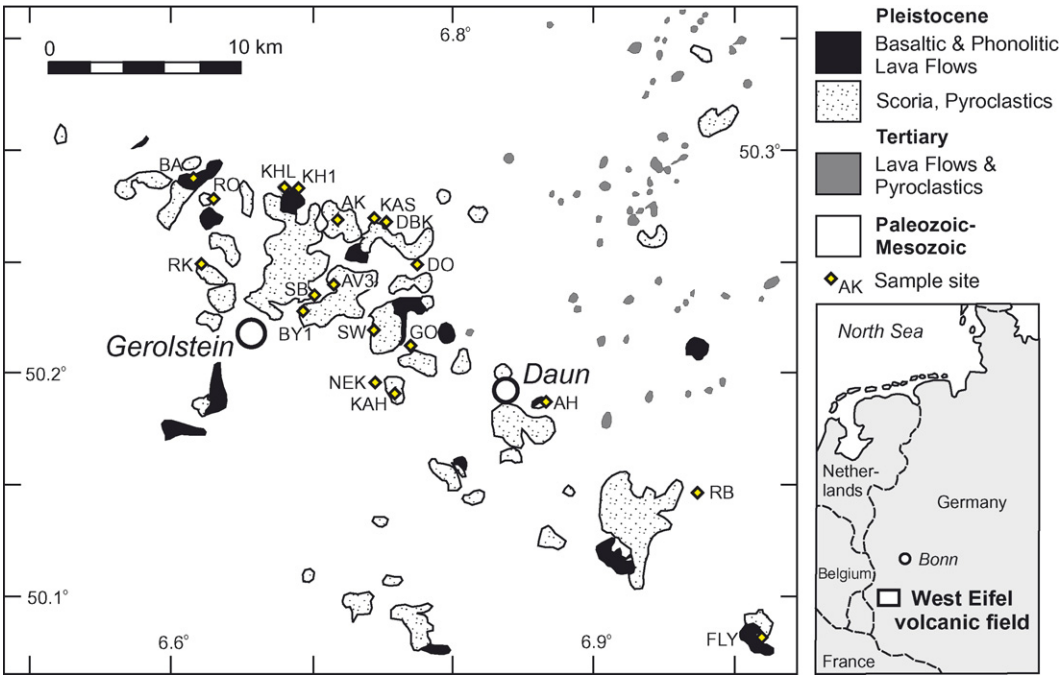

Fig. 1. Map of West Eifel volcanic field showing location of lava flow sites of Schnepp and Hradetzky (1994) dated as part of this study.

and are likely an intrinsic feature of geodynamo behavior during pre-Quaternary time as well. Indeed, knowing with precision the number, timing and duration of excursions is considered essential both to understanding geodynamo processes and to establishing global high-resolution correlation of relative paleointensity records in marine sediment. For example, Gubbins (1999) proposed that complete polarity reversals require a significant period, >3 kyr, for magnetic flux to escape from the solid inner core and sufficiently weaken its stabilizing effect, whereas excursions reflect much shorter and more frequent weakenings of the main dipole field in the liquid outer core. Thus the duration and frequency of excursions relative to full polarity reversals may provide insight about time constants of magnetic flux and the coupling between the inner and outer core. Moreover, the geometry and timing of excursional VGP positions or paths can be used to assess the role of the lower mantle in modulating non-axial dipole fields (Hoffman and Singer, 2004; Laj et al., 2006). Dating of excursions expressed as paleointensity minima in marine sediments cored at widely spaced localities by means of O isotope-based astrochronology or correlation to polar ice cores has begun to establish a globally correlated record of geomagnetic field instabilities (e.g., Guyodo and Valet, 1999; Channell et al., 2000; Laj et al., 2004; Channell, 2006). Notwithstanding, differences in the composition of sediment, rate of deposition, and regional differences in salinity and temperature of ocean water can lead to O isotope-based astrochronologic ages for particular excursions that contrast from site to site by several percent, or several kyr (e.g., Channell, 1999; Channell and Raymo, 2003; Stoner et al., 2002). Radioisotopic dating of lavas flows using the $^{40}Ar/^{39}Ar$ method provides an independent means of determining ages for excursions that can be used as geochronologic tie points and thus calibration of the global record of relative paleointensity and geomagnetic field instability during the Quaternary (Singer et al., 1999, 2002, 2004a; Singer, 2007).

At least seven excursions that occurred during the Bruhnes Chron are now well-documented including the Mono Lake (~32 ka), Laschamp (41 ka), Blake (120 ka) Iceland Basin (188 ka), Pringle Falls (211 ± 13 ka), Big Lost (579 ± 6 ka), and Stage 17 (670 ka) (Channell, 2006; Laj and Channell, 2007; Singer et al., 2008). Ages for the Mono Lake, Laschamp, Blake, Iceland Basin, and Stage 17 excursions are derived from O isotope-based astrochronologies for several marine sediment cores, whereas the ages for the Pringle Falls and Big Lost excursions are from an $^{40}Ar/^{39}Ar$ dated ash bed in transitionally magnetized lake sediment in Oregon (Singer et al., 2008) and transitionally magnetized lava flow sequences on the islands of Tahiti (Hoffman and Singer, 2004) and La Palma (Singer et al., 2002). In addition, Guillou et al. (2004) determined a radioisotopic age of 40.4 ± 1.1 ka for the Laschamp excursion based on unspiked K–Ar and $^{40}Ar/^{39}Ar$ dating of the Laschamp and Olby basalt flows in France. Beyond these well-known excursions, there are claims that several others occurred in the lower half of the Brunhes Chron between about 300 and 776 ka (e.g., Langereis et al., 1997; Lund et al., 2001a,b, 2006; Knudsen et al., 2003), but poor recordings – in many cases by only single specimens of sediment or lava flows – and imprecise geochronology, limit the utility of these records (Laj and Channell, 2007).

The Late Pleistocene West Eifel volcanic field, Germany, comprises dozens of small eruptive centers including scoria cones, lava flows, dikes, and plugs that have been the object of comprehensive campaigns by Böhnel et al. (1987) to determine paleodirections and the VGP distribution from 66 independent volcanic units and Schnepp (1992, 1994) who determined paleointensities from 37 of these units using a modified Thellier method. A dozen of the VGPs fall well outside of expected secular variation with latitudes <45°, but over a relatively restricted longitudinal zone including the Middle East and Southern Asia. This finding led Böhnel et al. (1987) to propose that several West Eifel volcanoes record a geomagnetic excursion. Schnepp and Hradetzky (1994) determined $^{40}Ar/^{39}Ar$ ages from seven of the excursional lava flows, but these measurements were only sufficiently precise at 95% confidence level to conclude that these lavas record geomagnetic excursion that occurred between about 570 and 450 ka, thus it has been impossible to correlate the excursional behavior recorded at West Eifel unequivocally with well-known excursions such as the 579 ± 6 ka Big Lost excursion, or other candidates tentatively identified in marine sediments (Lund et al., 2006).

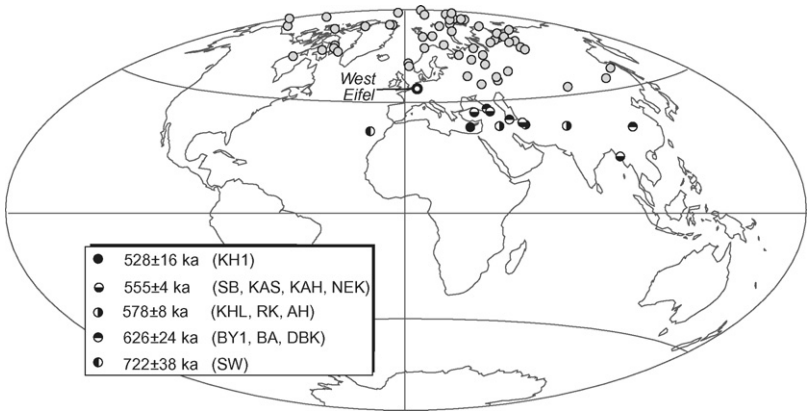

Fig. 2. VGP distributions of West Eifel volcanic units (data from Böhnel et al., 1987; Schnepp and Hradetzky, 1994). Samples with VGPs less than 45° that have been $^{40}Ar/^{39}Ar$ dated are denoted with symbols that illustrate clustering of ages into five groups. See text for discussion.

The goals of this study are to: (1) determine the timing of excursional behavior recorded in West Eifel lavas via precise $^{40}Ar/^{39}Ar$ dating methods, (2) review the record of Brunhes Chron excursions globally and, if possible, correlate the West Eifel excursion to marine sediment and other volcanic records, and (3) evaluate the recorded paleofield behavior in terms of controls on behavior of the geodynamo during excursions. Our findings indicate that multiple excursions are recorded in the West Eifel lavas and further that oscillatory shifts in the geometry and strength of the magnetic field over 200 kyr are consistent with a simple model whereby the lower mantle controls the non-axial dipole field during times when the dipole field is weakened.

2. The West Eifel volcanic field

The West Eifel volcanic field comprises more than 240 scoria cones, maars and small stratovolcanoes distributed throughout 600 km^2 southwest of Bonn, Germany (Fig. 1). The geology and petrology have been summarized in Büchel et al. (1986), Büchel (1994) and Shaw (2004). Schnepp (1994) also gave a brief summary and only the most salient points are mentioned here. These volcanoes and related intrusions comprise 6 km^3 that reflect melting within a mantle plume which produced magnesian nephelinite, leucitite and melilite magmas (Keyser et al., 2002). The eruptive centers are aligned in a southeast–northwest orientation (Büchel, 1994; Fig. 1). Radioisotopic dating using K–Ar, $^{40}Ar/^{39}Ar$, and ^{14}C methods indicates that volcanism began about 650 ka in the northwestern part of the field and that it migrated toward the southeast where the youngest eruptions occurred about 10 ka (Schmincke et al., 1983; Fuhrmann and Lippolt, 1987; Zöller, 1989; Schnepp and Hradetzky, 1994).

3. Paleomagnetic directions and intensities

Paleomagnetic measurements, including directions and VGPs from 91 sites in 66 volcanic units, and the results of absolute paleointensity experiments from 69 sites in 51 of these units are summarized in Schnepp and Hradetzky (1994). The paleodirections were obtained by Böhnel et al. (1987) using mainly step-wise alternating field (AF) demagnetization with maximum fields between 80 and 160 kA/m and in most cases resulted in single, primary magnetization components. Thirty percent of the 66 units yielded VGP latitudes lower than 60°N, but notably, 12 VGPs are lower than 45°N latitude and 8 of these are tightly clustered over the Middle East near 40°N latitude and 45°E longitude (Fig. 2).

Paleointensity experiments were carried out by Schnepp (1994) on 418 specimens using the Thellier method (Thellier and Thellier, 1959) as modified by Coe (1967); 312 of these experiments yielded acceptable results from 37 of the volcanic units including 10 of the units with low latitude VGPs (Schnepp and Hradetzky, 1994). Each of these experiments also yielded a paleodirection indistinguishable within α_{95} uncertainties from that of the same unit obtained by Böhnel et al. (1987). Unit mean paleointensities range from 7 to 62 μT with uncertainties commonly less than 10%. Virtual dipole moments (VDMs) calculated from the paleointensity measurements range from 1 to 10 × 10^{22} Am^2 and show a strong correlation with VGP latitude (Schnepp and Hradetzky, 1994; Fig. 3). Nine of the 12 lava flow sites with VGPs below 45°N latitude yielded paleointensities; all have VDM values of below 4, or less than half that of the present day field.

Böhnel et al. (1987) and Schnepp and Hradetzky (1994) proposed that the low latitude VGPs and low VDMs of the 12 West Eifel lava flows record an excursion of the geomagnetic field. The $^{40}Ar/^{39}Ar$ dating of seven of the excursional flows, and two of the flows with high latitude VGPs gave indistinguishable, but imprecise, results, leading Schnepp and Hradetzky (1994) to conclude that at some time during the lower Brunhes Chron between about 570 and 450 ka ($\pm 2\sigma$) the main dipole field weakened and a directional excursion resulted.

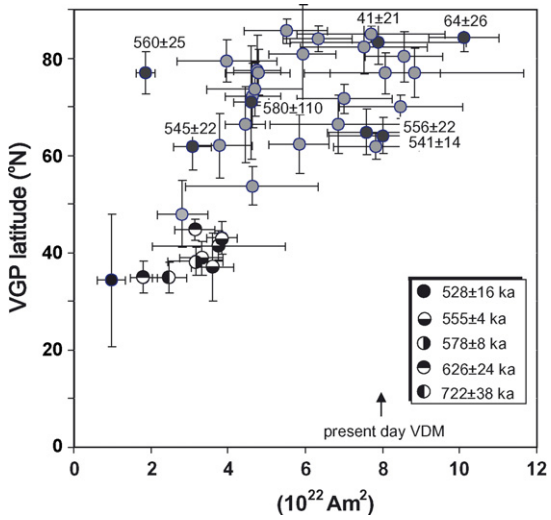

Fig. 3. Plot of VGP latitude vs. VDM values for West Eifel lava flows. Data from Schnepp and Hradetzky (1994). Symbols and $^{40}Ar/^{39}Ar$ ages of samples with VGPs less than 45° and VDMs less than 4 are same as in Fig. 2. See text for discussion of age groupings.

4. $^{40}Ar/^{39}Ar$ and K–Ar samples and analytical methods

From 19 lava flows, including the 12 excursional flows and 7 with high latitude VGPs, groundmass samples free of phenocrysts were prepared from 1-in. paleomagnetic cores that had been used for AF demagnetization. This was done by crushing, sieving to isolate the 180–250 μm fraction, passing a strong (Sm–Co) hand magnet over the sample to the attract iron oxide-rich groundmass, further separation of groundmass from any remaining olivine and pyroxene phenocrysts by graviational settling in heavy liquid (methylene iodide), and hand-picking under a binocular microscope (Singer et al., 2004b). Multiple aliquots of each sample weighing 93–140 mg were wrapped in 99.99% Cu foil packets and loaded into 2.5 cm diameter Al discs alongside 1.194 ± 0.012 Ma Alder Creek rhyolite sanidine (ACs) or, for the normally magnetized lava samples, both ACs and the 28.34 ± 0.16 Ma Taylor Creek rhyolite sanidine neutron fluence monitors that have been intercalibrated precisely against one another (Renne et al., 1998). For a small number of phenocryst-free samples 5 mm diameter by 1 mm thick wafers were drilled directly from the paleomagnetic core samples and were not wrapped in copper foil. Samples and flux monitors were co-irradiated for 60 or 90 min at the Oregon State University TRIGA reactor in the Cadmium-Lined In-Core Irradiation Tube (CLICIT). Correction factors for undesirable nucleogenic reactions are based on measurements of Ca- and K-free salts, including data collected at UW-Madison, and are: $[^{40}Ar/^{39}Ar]_K = 0.00086$; $[^{36}Ar/^{37}Ar]_{Ca} = 0.000264$; $[^{39}Ar/^{37}Ar]_{Ca} = 0.000673$ (Singer et al., 2004b).

Single crystals of the neutron flux monitors were fused with a 25 W CO_2 laser and their argon isotope composition was measured statically on a Balzers SEV-217 electron multiplier to calculate the neutron fluence, or J, values. Using a resistance furnace, the groundmass aliquots were degassed at 480 °C for 50 min to reduce atmospheric contamination, then incrementally heated to release the argon in 30–100° steps between 600° and 1300 °C and measured at UW-Madison using procedures detailed in Singer et al. (2004b). Five or more blanks spanning the temperature range utilized were measured between each sample and were at least an order of magnitude smaller than the samples. Mass discrimination was monitored by measuring the isotopic composition of purified atmospheric argon several dozen times during the two main analytical sessions and ranged from 1.0060 ± 0.0005 to 1.0069 ± 0.0005. Analytical uncertainties are calculated as in Singer et al. (2004b) and are reported at $\pm 2\sigma$, i.e., the 95% confidence level. Criteria for calculating plateau ages and the isochron from the plateau data are from Singer et al. (2004b). The isochron ages are preferred because they make no assumption regarding the trapped component.

For two of the excursional samples, NEK and AH, unspiked K–Ar ages were determined in addition to the $^{40}Ar/^{39}Ar$ ages as an independent cross-check on the results. The unspiked K–Ar ages were determined at Gif-sur-Yvette, France, following procedures fully documented in Singer et al. (2004b) and Guillou et al. (2004) that demonstrate close intercalibration between results from these two laboratories.

5. $^{40}Ar/^{39}Ar$ and unspiked K–Ar results

The results of 49 $^{40}Ar/^{39}Ar$ incremental heating experiments and 4 unspiked K–Ar experiments are summarized in Tables 1 and 2, respectively. Complete analytical details for the $^{40}Ar/^{39}Ar$ experiments are in Appendix. With the exceptions of two samples noted below, 33 of the 49 incremental heating experiments are nearly concordant such that 90% or more of the ^{39}Ar released in successive steps define an age plateau. Most other experiments are only slightly discordant with more than 70% of the ^{39}Ar defining a plateau age (Table 1). The $^{40}Ar/^{36}Ar$ intercepts of the isochron regressions indicate that excess argon is not present at significant levels in any of these 19 samples. The weighted mean $^{40}Ar/^{39}Ar$ isochron ages of the 12 excursional lava flows range from 722.0 ± 38.0 to 528.4 ± 16.0 ka, whereas those from the 7 normally magnetized lavas with high latitude VGPs range from 580.2 ± 109.6 to 41.0 ± 21.0 ka (Table 1). One exceptional sample is KHL which yielded a strongly discordant age spectrum in which only low temperature gas steps comprising 25% of the ^{39}Ar released define a plateau. This sample is by far the least radiogenic of those studied. Most gas increments contain only 1–3% radiogenic argon, thus the isochron is very poorly defined. Thus, for sample KHL we use the imprecise plateau age of 597.9 ± 135.0 ka with caution as a rough estimate for the age of this flow. This age is not used in calculations that attempt to subdivide temporal groupings discussed below. The second problematic sample is BA for which each of the three incremental heating experiments is strongly discordant, with a staircasing downward sequence of ages and K/Ca ratios from low to high temperature. Between about 36 and 62% of the gas released at the highest temperatures define "quasi-plateau" and isochron ages that are indistinguishable from one another. We interpret the discordant age spectra from sample BA as reflecting ^{39}Ar recoil in fine-grained glassy or altered domains within the groundmass. Notwithstanding, the consistent results from the high temperature portions of these experiments lead us to consider the weighted mean isochron of 629.0 ± 27.0 ka as a good estimate of the age of this lava flow. BY1 is among the less radiogenic samples; it yields a saddle-shaped age spectrum with 74% of the gas defining a plateau age of 584.2 ± 26.5 ka and an imprecise isochron that gives a preferred age for this lava of 629.7 ± 111.5 ka.

More typically, age spectra are nearly concordant with the precision of the isochron regressions a function of radiogenic argon contents that differ from sample to sample. For example in Fig. 4, each of the five subsamples from lava KAH yielded gas increments that typically contain 30–75% radiogenic argon, hence there is good spread of data points and the isochron based on regressing 59 plateau points has a precision of about 1%. In contrast gas increments from sample AH contain 10–35% radiogenic argon and the resulting isochron is about 3 times less precise than for sample KAH (Fig. 4). Sample DBK is more challenging still: the argon is only 3–10% radiogenic in each increment, thus there is little spread of data points along the isochron and it is only precise to about 9% (Fig. 4).

Replicate unspiked K–Ar experiments on samples KAH and AH yield weighted mean ages of 553.0 ± 12.0 and 583.0 ± 13 ka, respectively (Table 2). The unspiked K–Ar ages are in excellent agreement with the $^{40}Ar/^{39}Ar$ isochron ages of 555.2 ± 5.4 and 577.0 ± 16.0 ka obtained from samples KAH and AH, respectively (Fig. 4; Table 1). In addition to providing independent constraints on the timing of eruption of these two lavas, the K–Ar ages, together with the $^{40}Ar/^{39}Ar$ ages argue strongly that these two excursional flows erupted about 20 kyr apart, as will be discussed below.

The age determinations for the twelve excursional samples span nearly 200 kyr between about 722 and 528 ka and are listed along with the paleomagnetic directions and intensity data in Table 3. Five of the seven samples with high latitude VGPs yield isochron ages between 580.2 ± 109.6 and 541.0 ± 14.0 ka that are indistinguishable from one another and fall well within the age range of the excursional lavas (Fig. 5). Replicate experiments on two normally magnetized samples from the southeastern part of the volcanic field, FLY and RB, yield isochron ages of 64.0 ± 26.0 and 41.0 ± 21.0 ka (Table 3) indicating that they are much younger than other lava flows to the northwest, a finding consistent with that of Mertes and Schmincke (1983).

Table 1
Summary of 49 $^{40}Ar/^{39}Ar$ furnace incremental heating experiments of groundmass separates of West Eifel lava flows

Sample	Weight	K/Ca	Total fusion	Increments used	Age spectrum			*N*	Isochron analysis		
Experiment	(mg)	total	Age (ka) ± 2σ	°C	^{39}Ar (%)	MSWD	Age (ka) ± 2σ		$^{40}Ar/^{36}Ar_i$ ± 2σ	MSWD	Age (ka) ± 2σ
Transitionally magnetized lava flows											
KH1											
UW37B29 (wr)	130	0.061	539.8 ± 31.7	780–1350	100.0	0.40	527.9 ± 7.9	17 of 17	296.5 ± 1.8	0.35	528.4 ± 16.0
NEK											
UW37A17	101	2.879	587.1 ± 15.1	840–1150	73.9	1.43	560.0 ± 12.4	13 of 21	296.3 ± 5.7	1.55	555.5 ± 33.4
UW37A18	100	2.752	632.4 ± 32.7	830–1120	74.6	0.99	563.6 ± 10.2	8 of 15	297.5 ± 4.1	1.00	551.6 ± 26.8
UW50B1C	101	1.167	581.3 ± 12.5	570–1060	97.6	1.93	576.3 ± 15.0	14 of 15	300.4 ± 3.8	1.33	544.8 ± 27.5
UW50B2	108	0.862	585.7 ± 14.9	550–1040	95.7	0.94	573.2 ± 10.5	13 of 14	300.3 ± 4.0	0.49	542.4 ± 27.8
				weighted mean plateau age		1.50	567.7 ± 5.8	weighted mean isochron age		0.16	548.0 ± 14.0
KAH											
UW37A25 (wr)	120	2.986	539.0 ± 11.3	850–1200	92.0	0.42	547.9 ± 8.3	12 of 17	300.5 ± 10.2	0.36	542.3 ± 14.4
UW37A26 (wr)	140	2.175	546.8 ± 5.5	900–1140	86.8	2.12	547.3 ± 6.4	7 of 15	302.7 ± 8.6	1.91	541.8 ± 16.8
UW50D3	102	0.153	564.5 ± 8.3	660–1100	89.8	1.89	562.5 ± 8.2	11 of 14	299.5 ± 5.0	1.62	556.5 ± 10.9
UW50D3B	102	0.032	561.8 ± 8.5	580–1200	98.9	1.88	564.3 ± 8.5	14 of 15	295.6 ± 2.7	2.04	564.2 ± 10.4
UW50D2C	103	0.019	563.9 ± 12.7	550–1200	100.0	1.72	560.4 ± 9.1	15 of 15	298.4 ± 4.6	1.66	556.9 ± 10.7
				weighted mean plateau age		4.60	555.2 ± 3.5	weighted mean isochron age		2.20	555.2 ± 5.4
KAS											
UW37B33 (wr)	120	0.205	564.1 ± 20.5	820–1400	100.0	0.39	570.3 ± 17.1	17 of 17	295.0 ± 4.7	0.41	578.4 ± 34.7
UW37B34 (wr)	130	0.029	538.4 ± 26.8	780–1350	100.0	0.23	537.4 ± 19.8	14 of 14	295.3 ± 6.2	0.24	538.5 ± 39.3
UW50D5	100	0.103	571.9 ± 23.0	550–1150	93.8	0.14	546.4 ± 19.5	14 of 15	295.8 ± 3.9	0.15	543.7 ± 39.2
UW50D5B	103	0.052	556.9 ± 17.11	550–1200	100.0	0.24	556.9 ± 17.1	14 of 14	296.4 ± 3.0	0.24	549.0 ± 32.9
UW50D4C	99	0.013	563.3 ± 24.4	550–1200	100.0	1.08	556.0 ± 19.0	15 of 15	295.0 ± 2.2	1.15	562.5 ± 32.6
				weighted mean plateau age		0.38	553.0 ± 11.0	weighted mean isochron age		0.31	553.0 ± 20.0
SB											
UW37B31 (wr)	120	2.195	556.4 ± 10.0	850–1350	97.4	0.22	556.7 ± 9.7	15 of 17	297.2 ± 5.3	0.20	556.3 ± 17.5
UW50D1	100	0.027	560.9 ± 7.7	740–1200	86.8	0.25	555.6 ± 7.4	9 of 14	296.4 ± 4.2	0.26	555.1 ± 7.8
UW50D1B	102	0.024	564.3 ± 8.3	620–1200	99.6	1.59	562.8 ± 8.5	12 of 13	298.0 ± 4.8	1.59	560.1 ± 10.1
				weighted mean plateau age		0.88	558.2 ± 4.8	weighted mean isochron age		0.31	556.9 ± 5.8
AH											
UW37A19	111	0.065	573.9 ± 20.0	850–1400	100.0	1.25	584.0 ± 16.4	16 of 16	296.5 ± 2.8	1.28	573.5 ± 33.3
UW37A20	98	0.089	598.9 ± 22.1	850–1300	84.9	0.45	593.5 ± 13.9	14 of 17	294.6 ± 3.1	0.46	600.8 ± 31.7
UW50A5C	108	0.025	576.5 ± 22.9	570–1200	100.0	0.85	579.1 ± 14.8	14 of 14	297.2 ± 2.2	0.73	565.8 ± 23.3
UW50B4C	95	0.014	585.2 ± 51.9	550–1200	100.0	0.23	579.6 ± 33.3	14 of 14	295.8 ± 5.2	0.25	577.7 ± 51.7
				weighted mean plateau age		0.74	585.6 ± 8.3	weighted mean isochron age		1.07	577.0 ± 16.0
RK											
UW37A22	100	2.420	616.7 ± 28.3	880–1120	76.4	0.40	570.1 ± 8.1	9 of 18	296.6 ± 6.8	0.44	565.5 ± 29.7
UW50A3C	93	0.189	581.4 ± 14.2	570–1100	100.0	0.85	582.7 ± 11.9	13 of 13	295.8 ± 2.0	0.92	581.3 ± 16.1
UW50A4C	105	1.830	601.2 ± 17.4	570–860	86.0	1.23	583.4 ± 10.3	9 of 14	301.0 ± 4.6	0.55	540.2 ± 37.1
				weighted mean plateau age		2.70	576.9 ± 5.6	weighted mean isochron age		2.20	573.0 ± 13.0
KHL											
UW37A15	109	1.824	999.0 ± 81.9	790–1030	25.8	0.12	597.9 ± 135.0	13 of 21	293.2 ± 17.8	0.12	883.6 ± 1232.5
DBK											
UW37A13	104	0.202	603.7 ± 32.6	745–1400	100.0	0.35	608.6 ± 21.9	23 of 23	296.1 ± 3.2	0.36	596.6 ± 72.5
UW37A14	114	0.217	649.7 ± 38.6	830–1300	89.5	0.24	612.5 ± 25.0	11 of 13	294.8 ± 3.7	0.25	627.5 ± 82.5
UW50B4	98	1.122	656.3 ± 23.8	620–780	71.0	0.54	623.4 ± 25.7	5 of 13	297.1 ± 27.0	0.72	592.3 ± 438.7
UW50B3C	104	1.056	663.1 ± 29.7	570–780	75.2	0.79	633.2 ± 25.1	8 of 15	289.7 ± 14.5	0.82	738.5 ± 240.8
	weighted mean plateau age		0.86	619.0 ± 12.0	weighted mean isochron age		0.47	616.0 ± 53.0			

BA											
UW37A11	105	1.012	3347.0 ± 226.3	1230–1350	41.6	0.11	608.7 ± 20.4	3 of 14	283.6 ± 40.7	0.01	664.0 ± 241.5
UW37A12	1200	0.047	1273.7 ± 50.1	1200–1350	36.4	0.54	623.7 ± 14.0	4 of 14	292.5 ± 5.5	0.24	639.0 ± 31.9
UW50A1C	97	0.034	1729.0 ± 53.9	870–1200	62.5	8.60	601.9 ± 33.9	6 of 14	297.2 ± 11.5	10.69	597.5 ± 54.2
				weighted mean plateau age		1.19	617.0 ± 11.0	weighted mean isochron age		0.91	629.0 ± 27.0
BY1											
UW37A28 (wr)	135	1.336	673.3 ± 27.4	910–1200	74.3	0.19	584.2 ± 26.5	10 of 18	292.4 ± 7.4	0.12	629.7 ± 111.5
SW											
UW37A23	101	0.327	702.9 ± 49.9	820–1400	100.0	0.50	702.5 ± 25.1	14 of 14	295.2 ± 1.6	0.21	716.3 ± 46.2
UW37A24	101	0.442	770.1 ± 63.5	820–1300	90.4	0.14	727.0 ± 26.9	13 of 16	295.3 ± 2.1	0.04	732.8 ± 68.0
				weighted mean plateau age		1.80	714.0 ± 18.0	weighted mean isochron age		0.16	722.0 ± 38.0
Normally magnetized lava flows											
RO											
UW62C1	101	0.712	598.2 ± 74.6	770–1220	98.9	0.43	596.6 ± 46.3	8 of 10	296.1 ± 3.7	0.48	580.2 ± 109.6
AK											
UW62A1a	111	0.228	504.0 ± 17.9	750–1050	84.7	1.11	531.0 ± 14.3	7 of 11	297.1 ± 10.3	1.31	524.9 ± 41.8
UW62A1b	106	0.621	545.0 ± 23.7	660–1200	100.0	0.45	546.2 ± 19.6	12 of 12	294.1 ± 4.0	0.45	552.4 ± 26.3
				weighted mean plateau age		1.60	536.0 ± 12.0	weighted mean isochron age		1.20	545.0 ± 22.0
AV3											
UW62A3a	99	0.271	548.8 ± 34.4	750–1250	100.0	0.79	549.6 ± 23.6	110of 11	295.2 ± 1.9	0.87	552.7 ± 31.2
UW62A3b	108	0.397	546.8 ± 27.8	700–1220	99.8	0.62	549.5 ± 23.3	11 of 12	294.8 ± 1.6	0.60	559.5 ± 31.5
				weighted mean plateau age		0.00	550.0 ± 16.0	weighted mean isochron age		0.10	556.0 ± 22.0
GO											
UW62B3a	103	0.186	549.8 ± 35.8	780–2160	97.2	0.87	548.7 ± 27.6	12 of 13	295.0 ± 2.0	0.93	555.8 ± 38.5
UW62B3b	102	0.258	545.0 ± 30.5	700–1230	100.0	0.48	554.4 ± 22.8	11 of 11	294.8 ± 2.0	0.48	563.3 ± 33.7
				weighted mean plateau age		0.10	552.0 ± 18.0	weighted mean isochron age		0.09	560.0 ± 25.0
DO											
UW62A5a	105	0.229	550.2 ± 21.3	700–1220	100.0	0.45	547.3 ± 15.1	12 of 12	296.4 ± 2.7	0.45	542.8 ± 20.8
UW62A5b	106	0.286	536.9 ± 20.2	700–1220	99.3	0.46	540.8 ± 15.0	11 of 12	295.7 ± 3.9	0.51	540.2 ± 19.9
				weighted mean plateau age		0.37	544.0 ± 11.0	weighted mean isochron age		0.03	541.0 ± 14.0
FLY											
UW62B5a	108	0.175	147.1 ± 40.7	720–1220	100.0	1.14	115.5 ± 27.8	12 of 12	298.1 ± 2.6	0.84	82.4 ± 33.8
UW62B5b	110	0.304	91.0 ± 34.8	650–1200	100.0	0.44	74.6 ± 30.2	11 of 11	298.3 ± 3.1	0.10	35.6 ± 42.4
				weighted mean plateau age		4.00	97.0 ± 20.0	weighted mean isochron age		3.00	64.0 ± 26.0
RB											
UW62B1a	112	0.200	138.0 ± 45.9	730–1220	99.8	3.01	89.8 ± 37.6	11 of 12	297.2 ± 2..3	2.69	58.8 ± 31.9
UW62B1b	106	0.188	88.3 ± 88.9	650–1240	100.0	0.47	47.5 ± 30.2	10 of 10	296.6 ± 1.8	0.34	28.3 ± 27.0
				weighted mean plateau age		3.10	64.0 ± 24.0	weighted mean isochron age		2.10	41.0 ± 21.0

All ages calculated using the decay constants of Steiger and Jäger ($\lambda_{40K} = 5.543 \times 10^{-10}$ year^{-1}).
J-values for transitional lavas calculated relative to 1.194 Ma Alder Creek rhyolite sanidine. *J* values for normally magnetized lavas calculated relative to both 28.34 Ma Taylor Creek rhyolite and 1.194 Ma Alder Creek rhyolite sanidine. These two neutron fluence monitors have been precisely intercalibrated by Renne et al. (1998).
(wr) = whole-rock.

Table 2
Summary of unspiked K–Ar experiments on groundmass of West Eifel lava flows

Sample experiment	Weight molten (g)	K (wt.%)	$^{40}Ar^*$ (%)	$^{40}Ar^*$ ($\times 10^{-12}$ mol/g)	Age $\pm 2\sigma$[a] (ka)
KAH					
7201	1.77233	2.806 ± 0.028	30.281	2.676	
7217	2.01430	2.806 ± 0.028	28.028	2.709	
Weighted mean				2.693 ± 0.020	553 ± 12
AH					
7200	1.05918	2.972 ± 0.029	16.602	2.948	
7215	1.54319	2.972 ± 0.029	22.639	3.046	
Weighted mean				3.004 ± 0.024	583 ± 13

[a] Ages calculated using decay constants of Steiger and Jäger (1977).

6. Discussion

6.1. Timing of excursional behavior recorded in West Eifel lavas

Our new $^{40}Ar/^{39}Ar$ age determinations are more precise than those obtained by Schnepp and Hradetzky (1994) for two reasons. First, experiments at UW-Madison were done on groundmass samples more than 10 times smaller by using an electron multiplier, rather than Faraday cage to detect argon ions, thus each subsample we measured was thoroughly hand-cleaned, is exceptionally homogeneous, and free of potential xenocrysts or altered phases. Second, we undertook replicate experiments on most samples, and for several samples as many as five or six experiments were done; the pooled results used to calculate the weighted mean isochron ages minimize random errors and lower the analytical uncertainties (e.g., Singer et al., 2004b; Guillou et al., 2004).

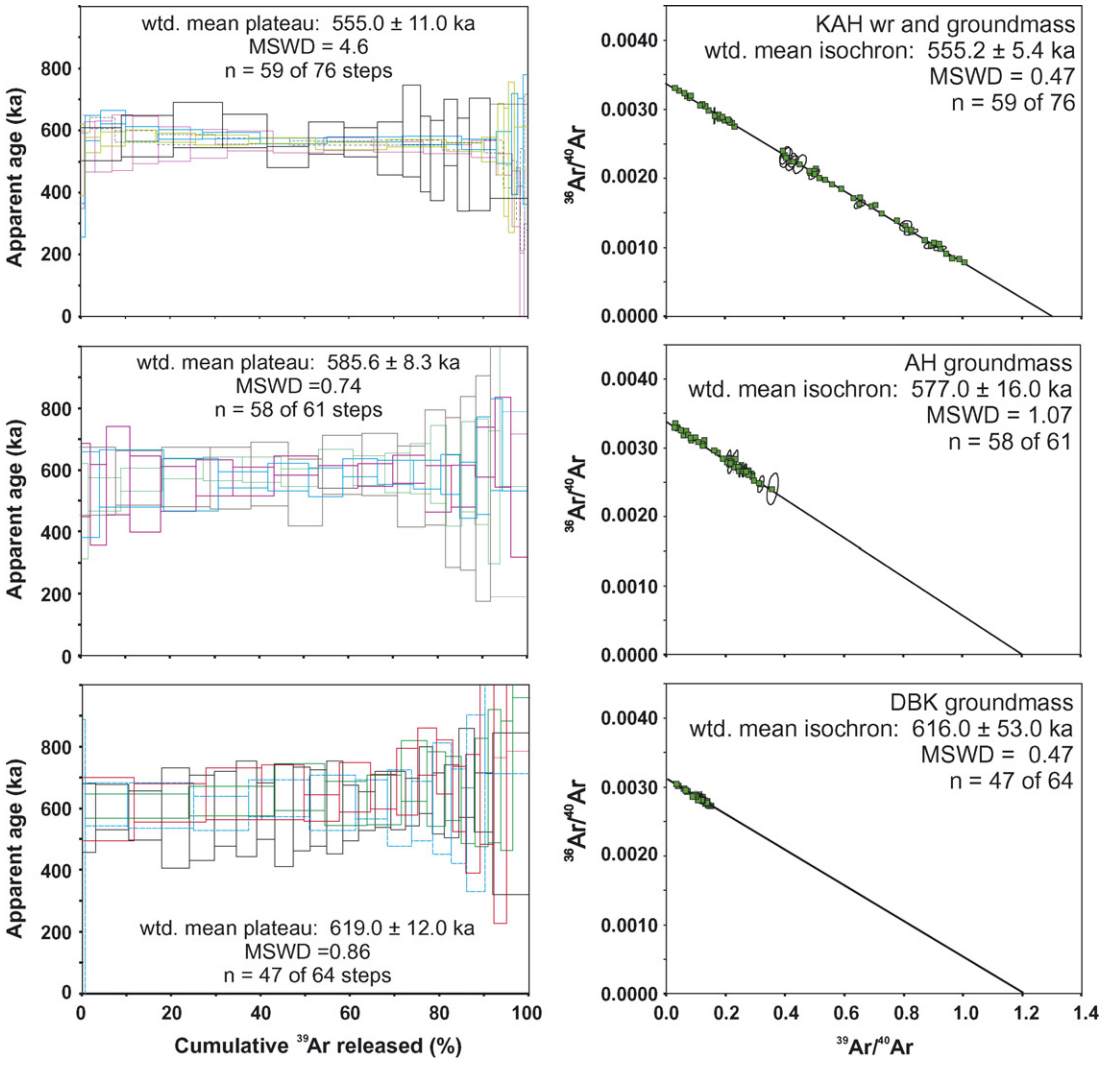

Fig. 4. Age spectrum and inverse isochron diagrams illustrating $^{40}Ar/^{39}Ar$ results from excursional lava flow samples KAH, AH, and DBK. In each case the isochron is calculated as the weighted mean of the isochrons from each separate experiment and the composite figure illustrates reproducibility between subsamples. The isochron ages give the best estimate of time since these lava flows were erupted; see text for discussion.

Table 3
Summary of paleodirection, paleointensity, and age data from 19 West Eifel lava flow sites

Site	Site lat. (°N)	Site long. (°E)	Declination (°)	Inclination (°)	α_{95} (°)	VGP lat. (°N)	VGP long. (°E)	$B_p \pm 1\sigma$ (μT)	VDM $\pm 1\sigma$ ($\times 10^{22}$ Am^2)	Age $\pm 2\sigma$ (ka)
KH1	50.281	6.690	123	78	7.8	34.3	30.6	7.1 ± 1.3	0.98 ± 0.36	528 ± 16
NEK	50.197	6.750	103	79	1.6	41.5	34.8	27.6 ± 6.4	3.76 ± 1.72	548 ± 14
KAH	50.192	6.761	92	76	2.0	43.1	43.4	27.5 ± 1.4	3.84 ± 0.39	555 ± 5
KAS	50.270	6.748	91	69	4.9	37.0	57.2	23.5 ± 1.7	3.59 ± 0.55	553 ± 20
SB	50.234	6.702	80	31	8.2	19.5	93.8	*nd*	*nd*	557 ± 6
AH	50.187	6.867	98	74	2.1	38.9	45.1	23.2 ± 2.0	3.31 ± 0.56	577 ± 16
RK	50.249	6.623	91	71	2.0	38.3	53.9	21.2 ± 2.4	3.16 ± 0.72	573 ± 13
KHL	50.283	6.684	80	59	6.0	37.5	79.4	*nd*	*nd*	598 ± 135
DBK	50.267	6.756	90	78	1.3	44.8	41.4	22.7 ± 1.9	3.14 ± 0.53	616 ± 53
BA	50.289	6.620	91	73	3.1	40.1	50.9	*nd*	*nd*	629 ± 27
BY1	50.229	6.699	57	33	5.1	35.0	110.9	7.9 ± 0.8	1.80 ± 0.35	630 ± 112
SW	50.220	6.749	238	78	1.8	34.9	342.6	17.9 ± 1.6	2.47 ± 0.44	722 ± 38
RO	50.277	6.631	15	79	6.5	70.9	24.1	33.6 ± 1.4	4.60 ± 0.47	580 ± 110
AK	50.265	6.714	47	77	2.8	61.9	47.3	22.1 ± 1.7	3.07 ± 0.48	545 ± 22
AV3	50.242	6.713	42	73	3.0	64.8	62.0	52.2 ± 3.4	7.58 ± 1.00	556 ± 22
GO	50.211	6.771	16	62	3.7	77.0	123.0	11.1 ± 0.7	1.85 ± 0.25	556 ± 25
DO	50.249	6.778	39	65	2.9	64.1	90.2	49.7 ± 4.3	8.01 ± 1.39	541 ± 14
FLY	50.082	7.019	5	64	2.2	84.2	152.7	62.0 ± 2.7	10.12 ± 0.91	64 ± 26
RB	50.149	6.976	12	68	4.0	82.4	86.6	48.7 ± 5.3	7.52 ± 1.65	41 ± 21

Paleomagnetic data from Schnepp (1994) and Schnepp and Hradetzky (1994). Ages from Table 1.

The ^{40}Ar/^{39}Ar ages of the 12 excursional flows span nearly 200 kyr, thus these lavas do not record a single excursion. A probability density distribution that takes into account the uncertainties on each individual age determination was calculated using ISOPLOT (Ludwig, 2003) and is illustrated in Fig. 5. The key feature revealed by the probability analysis is that between 800 and 500 ka there are five periods in which the ^{40}Ar/^{39}Ar age determinations are clustered and distinct from one another. The most prominent peak in the probability density plot is defined by the ^{40}Ar/^{39}Ar and K–Ar ages of samples NEK, KAH, KAS and SB which are indistinguishable from one another at the 95% confidence level. The variance weighted mean age of these four lavas is 555 ± 4 ka. Similarly, the subsidiary peaks are defined by the weighted mean of ages of 578 ± 8 ka from samples AH and RK, and 626 ± 24 ka from flows DBK, BA, and BY1. The remaining local maxima in probability are due to isochron ages of 528 ± 16 ka for sample KA1 and 722 ± 38 ka for sample SW (Table 3). These findings suggest that perhaps as many as five separate excursions are recorded by the lava flows in the West Eifel volcanic field.

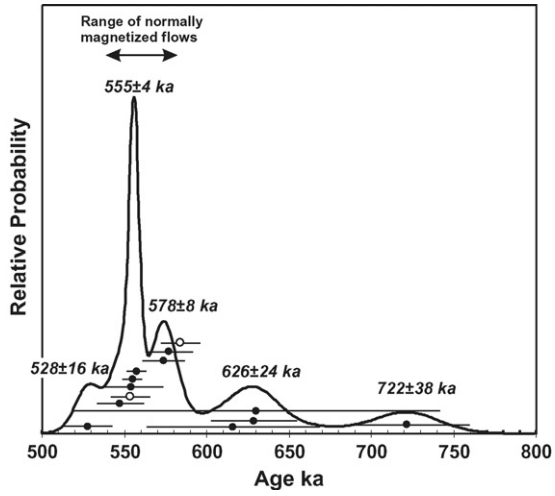

Fig. 5. Probability density plot calculated from the distribution of 11 ^{40}Ar/^{39}Ar ages of excursional lava flows. ^{40}Ar/^{39}Ar ages from individual samples shown as filled symbols, unspiked K–Ar ages are open symbols, each with ±2σ analytical uncertainty.

Five of the samples found to have high latitude VGPs, four of which have VDMs greater than 4 (Fig. 3), yield ages of between about 580 and 540 ka (Table 3) that span at least two of the age groups of excursional lava flows (Fig. 5). Thus, during the period from about 600 to 500 ka the geodynamo underwent at least three oscillations between a state characterized by a relatively strong dipole field and high latitude VGPs greater than 70° and one having much lower strength and VGPs below 45°. The excursional lavas SW and KH1 dated at ~722 and 528 ka further suggest that this oscillatory behavior may have occurred for nearly 200 kyr.

If, as proposed by Gubbins (1999), excursions are significantly shorter-lived features of paleofield behavior than full polarity reversals, then it is somewhat surprising to find that 18% of the 66 measured lavas in the West Eifel volcanic field record excursional field directions during a 200 kyr period. If all excursions are completed in only 1–2 kyr, as for example the GLOPIS-75 and ODP site 919 marine records suggest for the Laschamp and Mono Lake excursions (Laj et al., 2004; Channell, 2006), it seems highly improbable that so many West Eifel lavas would record five excursions that in total may account for <10 kyr of time. In contrast, the most detailed record of the Pringle Falls excursion in ODP site 919 sediments suggests that several large directional swings took place over nearly 20 kyr between 225 and 205 ka (Channell, 2006). Whether some excursions in the lower Brunhes chron are comparable in duration to the Pringle Falls excursion, or the Matuyama–Brunhes polarity reversal, which lasted perhaps 18 kyr (Singer et al., 2005), governs the probability that West Eifel lavas would record them. Many excursions lasting >10 kyr each would argue that Gubbins' (1999) hypothesis does not apply in general and that the mechanism for some excursions may be more similar to that for reversals – decay of the inner core-held field over several kyr – than proposed. An alternative hypothesis, introduced by Singer et al. (2008), proposes that this particular 200 kyr period is characterized by low field intensity and an unstable dynamo such that frequent oscillations in axial dipole strength and therefore numerous short-lived excursions are to be expected. Perhaps several additional excursions, each lasting no more than 2 kyr, during this interval are not recorded by West Eifel lavas? Testing these alternative hypotheses will require additional high-resolution paleomagnetic recordings coupled with further precise age control.

6.2. Excursions in the lower Brunhes Chron

The number and timing of excursions in the lower half of the Bruhnes Chron remains controversial and confusing, in part because several recordings in marine sediment do not have adequate chronological resolution and volcanic records are few (Laj and Channell, 2007). Champion et al. (1988) proposed that in addition to the Big Lost excursion initially defined by K–Ar dating of a transitionally magnetized basalt flow in Idaho 565 ± 28 ka (2σ), at least seven other excursions are recorded by sediment or lava flows during the Brunhes Chron. This list grew larger as Langereis et al. (1997) documented evidence for four short excursions in a piston core from the Mediterranean which they called the Calabrian Ridge 0 (CR0), CR1, CR2, and CR3 excursions, the latter possibly corresponding in age to the Big Lost excursion of Champion et al. (1988). Limited age control and the fact that the Calabrian Ridge excursions are defined only by single samples, have led some to question whether the CR excursions should be adopted into the calendar of Brunhes Chron excursions (Laj and Channell, 2007). Thus, as of a decade ago, based mainly on the reviews by Champion et al. (1988) and Langereis et al. (1997), the list of potential Brunhes Chron excursions included 12 (Fig. 6A).

Advances in the coring of long sequences of marine sediment deposited at high rates by the DSDP and ODP beginning in the early 1990s using a hydraulic piston corer facilitated the discovery of many new recordings of brief excursions (Laj and Channell, 2007). Initial studies of cores raised from North Atlantic sediment drifts during ODP leg 172 led Lund et al. (1998) to propose 14 plausible Brunhes Chron excursions, a number that Lund et al. (2001a,b) revised to 12 on the basis of more detailed measurements (Lund et al., 2006; Fig. 6B). The findings of Lund et al. (2001b) indicate that excursions are an intrinsic component of the geomagntic field and suggest that excursions occur temporally clustered in "bundles" of two or three separated by regular secular variation (Fig. 6B). However, a problem with the leg 172 cores is that continuous oxygen isotope-based astrochronology has not been done, thus it remains difficult to correlate the 12 or more excursions precisely to other independent records (Laj and Channell, 2007). Nonetheless, Lund et al. (2001a) recognized at least three, and possibly four, excursions between approximately 700 and 500 ka that are numbered 14α, 15α, 15β, and 17α denoting the oxygen isotope stages in which each is recorded (Fig. 6B). The 17α excursion may correspond with the "Stage 17" or Delta event found by Biswas et al. (1999) in sediments at Osaka Bay that is ca. 670 ka based on correlation with an excursion that is astronomically dated in ODP cores 980, 983, and 984 (Channell and Raymo, 2003; Channell et al., 2004; Laj and Channell, 2007).

Perhaps the most highly resolved and best-dated marine sediment sequence of the lower Brunhes Chron comes from ODP sites 983 and 984 where Channell et al. (2004) developed a continuous O-isotope astrochronologic age model, in addition to determining the inclination, declination, and relative paleointensity proxy records using u-channel samples. Between the base of the Brunhes Chron which has been dated at 776 ± 2 ka using ^{40}Ar/^{39}Ar (Coe et al., 2004; Singer et al., 2005) and 500 ka, the ODP site 983 and 984 sediments record three directional swings with VGPs crossing the equator at about 670, 590, and 540 ka (Channell et al., 2004; Fig. 6C). Channell et al. (2004) correlated these excursions with the Delta (Stage 17), "La Palma" and Big Lost excursions, respectively, each of which occurred during a period of low paleointensity found not only in the site 983 and 984 sediment, but also in the global stack of 33 sediment cores averaged by Guyodo and Valet (1999) (Fig. 6D).

Basaltic lava sequences on La Palma and Tahiti that possess similar excursional VGP paths over Asia and Australasia have been ^{40}Ar/^{39}Ar-dated at 580 ± 8 and 579 ± 9 ka by Singer et al. (2002) and Hoffman and Singer (2004) and are thought to record the Big Lost excursion of Champion et al. (1988). The weighted mean age of the excurional lavas from La Palma and Tahiti is 579 ± 6 ka, which is indistinguishable at the 95% confidence level from original whole-rock K–Ar age of 565 ± 28 ka (Champion et al., 1988) and the later ^{40}Ar/^{39}Ar age determination of 558 ± 20 ka (Lanphere, 2000; ±2σ uncertainties) for the lava flow in Idaho near the namesake Big Lost River (see Singer et al., 2002 for details). Thus the "La Palma" excursion recorded in ODP site 983 and 984 sediments by Channell et al. (2004) is best correlated with the Big Lost excursion on land and for reasons given by Singer et al. (2002) the term "La Palma" excursion should be abandoned. As will be discussed below, the Big Lost excursion is expressed globally in many lava flows and marine sediment cores and its radioisotopic age is 579 ± 6 ka (Hoffman and Singer, 2004; Singer, 2007).

Our findings indicate that as many as five temporally resolvable excrusions are recorded by lava flows of the West Eifel volcanic field. The most precisely dated of these excursions occurred at 555 ± 4 and 578 ± 8 ka, the latter is identical in age to the Big Lost excursion in the ^{40}Ar/^{39}Ar-based Geomagnetic Instability Time Scale (GITS) of Singer et al. (2002) and Singer (2007) (Fig. 6E), hence we correlate these excursional lavas with those at La Palma, Tahiti, and Idaho described earlier. Within the framework of the GITS, we informally designate the West Eifel excursions as West Eifel 1 (722 ka), West Eifel 2 (626 ka), Big Lost (579 ka), West Eifel 4 (555 ka), and West Eifel 5 (528 ka) (Fig. 6E). The Big Lost excursion occurs between plausible excursions 15α and 15β of Lund et al. (2006; Fig. 6B) and most closely correlates with the excursion and paleointensity low called "La Palma" by Channell et al. (2004) and Guyodo and Valet (1999) (Fig. 6). The West Eifel 4 occurs between plausible excursions 14α and 15α, whereas West Eifel 5 may correlate with the excursions called 14α (Lund et al., 2006) or the "Big Lost?" (Channell et al., 2004) (Fig. 6). West Eifel 4 and 5 coincide with a pair of global paleointensity lows in the SINT-800 curve of Guyodo and Valet (1999) (Fig. 6C and E). The excursions we call West Eifel 1 and 2 are less precisely dated and may correlate with excursions 17α and 15β, respectively, but not with the Delta event as documented by Channell et al. (2004) in the ODP site 983 and 984 cores (Fig. 6). However, there are local minima in the global paleointensity curve of Guyodo and Valet (1999) during which these West Eifel excursions could have occurred given the large uncertainties of the ^{40}Ar/^{39}Ar ages (Fig. 6). We tentatively correlate the West Eifel 2 excursion with 15β of Lund et al. (2006) (Fig. 6). However, until a more precise age can be determined from lava site SW, or additional high-resolution sediment cores are characterized, verification and correlation of the West Eifel 1 excursion remains speculative.

More clearly, the period of time between about 620 and 520 ka is characterized globally by remarkably low average paleointensity, during which the four youngest West Eifel excursions were recorded (Fig. 6), possibly reflecting a "bundle" according to Lund et al. (1998). The GITS for the lower Brunhes Chron between 776 and 500 ka now includes at least five well-documented excursions including the Stage 17 (670 ka), West Eifel 2 (626 ka), Big Lost (579 ka), West Eifel 4 (555 ka) and West Eifel 3 (528 ka) excursions (Fig. 6E). Considering the GITS for the entire Brunhes Chron, there is compelling evidence for at least 10, and possibly 11 excursions. Precise radioisotopic ^{40}Ar/^{39}Ar ages have been obtained for six of these excursions (Fig. 6E).

6.3. Mechanism for oscillatory excursions

The fact that the five temporally resolvable excursions are associated with similar paleodirections, and hence, similar VGPs, is both remarkable and not likely to be fortuitous. It is more prob-

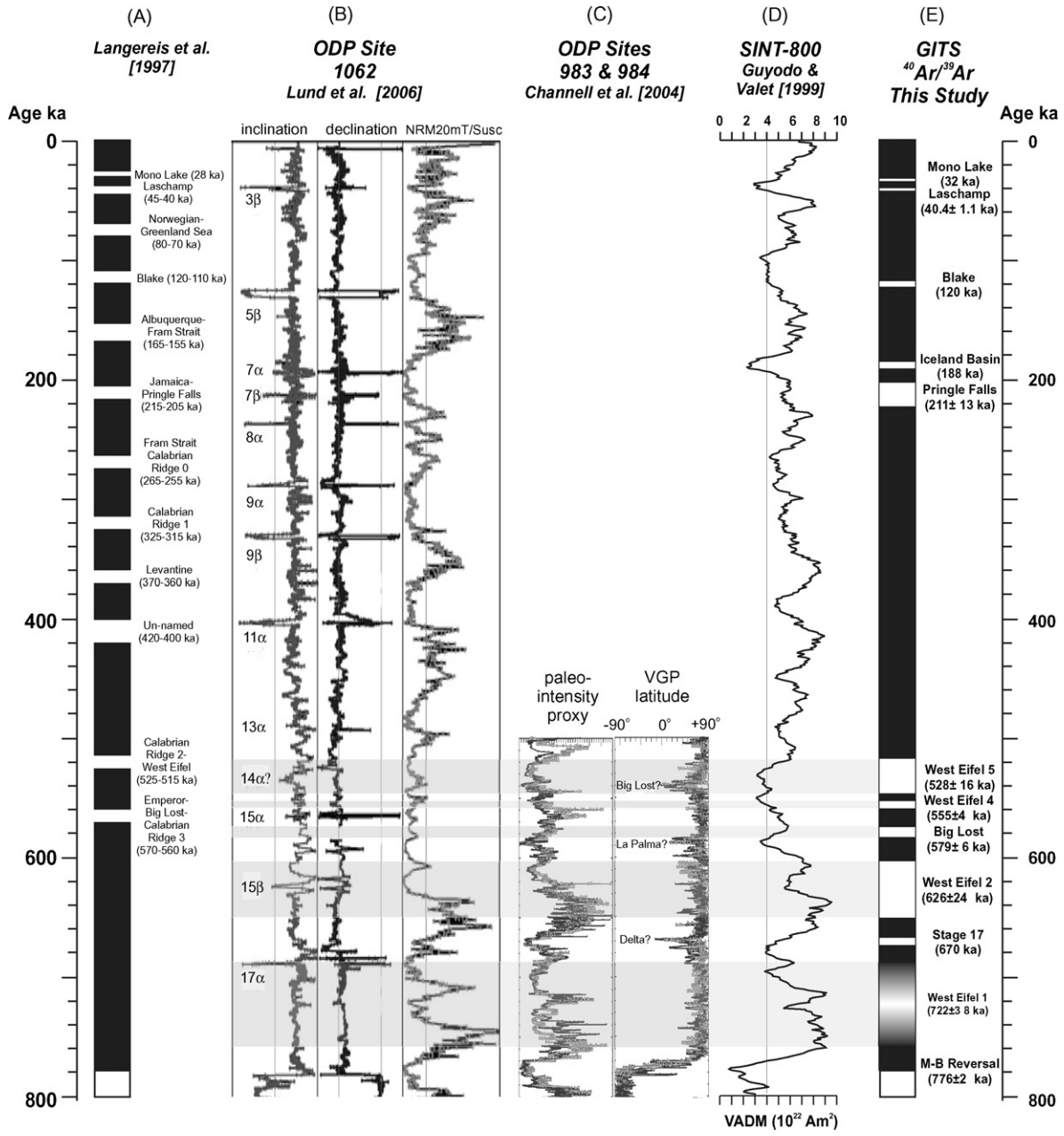

Fig. 6. Records of geomagnetic excursions and paleointensity in the Brunhes Chron. Records are from: (A) Langereis et al. (1997), (B) Lund et al. (2006), (C) Channell et al. (2004), (D) Guyodo and Valet (1999), and (E) Geomagnetic Instability Time Scale (GITS) based on $^{40}Ar/^{39}Ar$-dated volcanic rocks discussed in the text (Singer et al., 2002, 2005; in review; Singer, 2007), plus excursions in marine sediment cores that have been dated via continuous O isotope-based astrochronology (e.g., Channell et al., 2004). See text for discussion.

able that these excursional data reflect similar field configurations, at least on a regional scale. If so, they provide important support to the contention that control by the lowermost mantle during times of weakened field intensity is paleomagnetically observable (e.g., Laj et al., 1991; Hofffman, 1992), and further, that the dynamo process responsible for such significant reductions in field strength is, in a manner of speaking, "simple". That is, recurring paleofield directions are associated with a recurring dynamo process. Hillhouse and Cox (1976) first suggested the possibility that transitional behavior could be dominated by standing field elements. Here we argue further that the least complicated way in which a field may "stand" over a geologic span of time is through the combined effect of an unstable axial dipole, one which experiences a series of collapses each separated by regenerations, and a quasi-static mantle-held non-axial dipole (or NAD) field.

This model has been successfully applied to the five presently available Plio-Pleistocene transitional fields recorded in lavas that were erupted at the Society Island hotspot (Hoffman and Singer, 2004). Displayed in these five records, including one corresponding to the Big Lost excursion at 579 ka, is an early clustering of VGPs found off the west coast of Australia; the location of this recurring cluster is well-simulated by the modern-day *south* VGP experienced at this site, given the total demise of the axial dipole. More specifically, the VGPs associated with the year 1900, 1950, and 2000 NAD-fields show little variation, all three situated near the paleomagnetically derived virtual poles along the west coast of Australia (Fig. 7A; Hoffman and Singer, 2004).

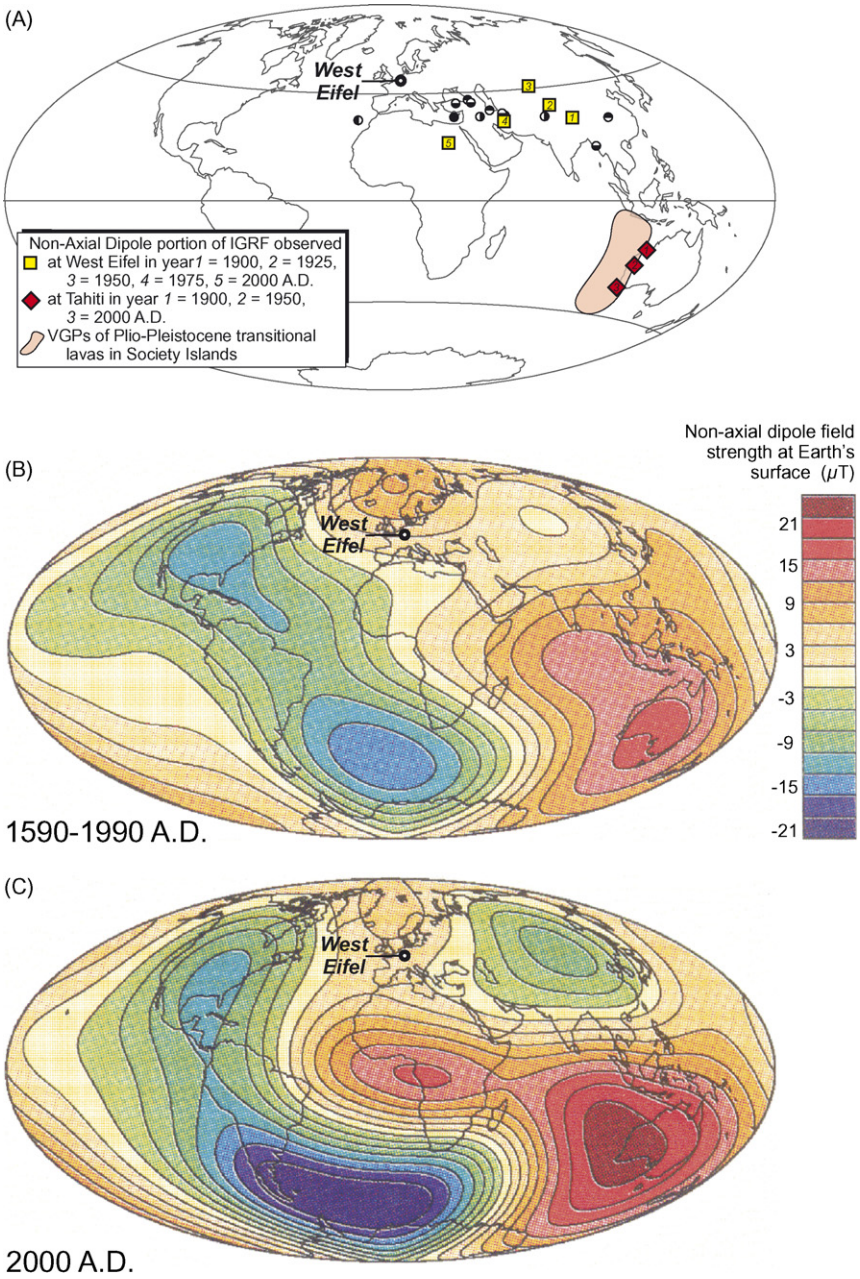

Fig. 7. (A) Excursional VGPs associated with multiple dynamo instabilities recorded in the West Eifel lava flows (symbols as in Fig. 2) and in lava flows in the Society Islands (red area). South VGPs associated with the non-axial dipole (NAD) field calculated from the IGRF at West Eifel (yellow squares) and Tahiti (red diamonds). (B and C) Vertical component of the NAD field estimated at the Earth's surface. (B) Averages the time dependency of the NAD field over 400 years between 1590 and 1990 A.D., based on the GUFM model of Jackson et al. (2000). (C) The Oersted secular variation model (OSVM) for year 2000 A.D. of Olsen (2002). Panels B and C modified from Constable (2007).

The fact that the Big Lost excursion is also recorded in the West Eifel volcanics offers the opportunity to further test the same modern-day field model. Note first that the West Eifel poles are mainly found in Eurasia strung about a significant range of longitude (cf. Figs. 2 and 7A). Also plotted in Fig. 7A are the south VGPs associated with the site for the same temporal range of modern-day NAD-fields, specifically, for the years 1900, 1925, 1950, 1975, and 2000. Interestingly, these five modeled VGPs also display a similar expanse of longitude as do the West Eifel paleomagnetic data. We interpret these findings from West Eifel lavas as adding significant support for the notion that dipole collapse is the first effect projected by an unstable dynamo (Singer et al., 2005), and that the residual field (i.e. the NAD-field) has altered little, apart from sign, over the time spanning these events. Similar conclusions were drawn by Glen et al. (1994, 1999)) from persistent features found in successive polarity transition records spanning the past ~15 Myr in western North America.

We also offer an explanation as to why it is that transitional field VGP clusters associated with recordings from the Society Island are so tightly amassed, whereas the multiple excursion data from West Eifel are more dispersed. We argue that the answer is seen in the NAD-field modeling over just 100 years of time. The two strongest NAD-field features observed at the Earth's surface during the past 500 years reside in the Southern Hemisphere (Fig. 7B) and during the past one hundred years these have been found to vary in relative significance while remaining spatially fixed (e.g.,

compare Fig. 7B and C; Hoffman and Singer, 2004). The degree to which the NAD field is altered upon collapse of the dipole field is therefore site-dependent and is strongly a function of the quasi-independent temporal variation in strength of the main NAD-field features. For the case of the Northern Hemisphere site of the West Eifel volcanic field, considerably distant from both of the Southern Hemisphere NAD field concentrations (Fig. 7), the effect appears to have been quite pronounced. Hence, this simple model, thus far applied to data from transitioanlly magnetized lavas obtained from two nearly antipodal sites, not only has been successful in its simulation of the respective locations of quasi-stationary, transitional VGPs, but also appears to explain the focused vs. longitudinally dispersed characteristics of the field behavior.

7. Conclusions

$^{40}Ar/^{39}Ar$ dating of 19 lava flows from the West Eifel volcanic field that record weak excursional and typical normal paleomagnetic fields indicate that at least 4 and possibly 5 excursions occurred between about 722 and 528 ka. These excursions correlate with the Big Lost excursion, previously $^{40}Ar/^{39}Ar$ dated at 579 ± 6 ka, and most probably with excursions expressed differentially in high deposition-rate sediments recovered via the ODP and known as plausible excursions 14α, 15α, and 15β (Lund et al., 2001a, 2006). Our findings indicate that the Brunhes Chron is characterized by at least 10 and possibly 11 excursions that are well-recorded and dated in marine sediments using O isotope-based astrochronology or in lava flows that have been $^{40}Ar/^{39}Ar$-dated. The excursions recorded by West Eifel lavas have VGPs that fall over the Middle East and South-central Asia. For one of these, the Big Lost excursion, the location of the VGPs from West Eifel is broadly similar to the VGP cluster derived from lavas on La Palma. However, they are clearly distinct from the VGP cluster recorded in Tahitian lavas. Provided the three clustered locations are indeed synchronous, the Big Lost transition field must contain a significant non-dipolar component.

The paleofield at West Eifel oscillated several times between normal polarity with typical strength, and a weak transitional field having longitudinally dispersed directions remarkably similar to those associated with the *south* VGPs calculated for the West Eifel site for the NAD-field during the 20th century. A model in which the axial dipole repeatedly collapses leaving behind a residual NAD-field that is largely held by stationary sources, in the lowermost mantle, provides a simple explanation for the recurrent excursional behavior during this ~200 kyr period.

Acknowledgements

Singer and Hoffman wish to express our most sincere thanks to Rixiang Zhu and Keke Zhang for inviting us to participate in a most memorable and stimulating meeting on Paleomagnetism and the Earth's Deep Interior. Reviews by Rob Coe and Fei Wang helped us improve the manuscript and are much appreciated. Singer wishes also to acknowledge laboratory assistance from Bill Cassata and Xifan Zhang. Jörg Negendank, GFZ Potsdam, provided financial support to archive the West Eifel paleomagnetic samples in the Eifelmuseum. This study was supported by U.S. NSF grants EAR-033768403 and EAR-0516760 to Singer and EAR-0230347 to Hoffman.

Appendix A. Supplementary data

Supplementary data associated with this article can be found, in the online version, at doi:10.1016/j.pepi.2008.05.001.

References

Biswas, D.K., Hyodo, M., Taniguchi, Y., Kaneko, M., Katoh, S., Sato, H., Kinugasa, Y., Mizuno, K., 1999. Magnetostratigraphy of Plio-Pleistocene sediments in a 1700-m core from Osaka Bay, southwestern Japan and short geomagnetic events in the middle Matuyama and early Brunhes chrons. Palaeogeogr. Palaeoclimat. Palaeoecol. 148, 233–248.

Böhnel, H., Reisman, N., Jäger, G., Haverkamp, U., Negendank, J.F.W., Schminke, H.-U., 1987. Paleomagnetic investigation of Quaternary West Eifel volcanics (Germany): Indication for increased volcanic activity during geomagnetic excursion/event? J. Geophys. Res. 62, 50–61.

Büchel, G. (Ed.), 1994. Vulkanologische Karte West- und Hocheifel. Landesvermessungsamt Rheinland-Pfalz, Mainz.

Büchel, G., Lorenz, V., Schmincke, H.-U., Zimanowski, B., 1986. Quartäre Vulkanfelder der Eifel. Fortschr. Miner. 64, 97–141.

Champion, D.E., Lanphere, M.A., Kuntz, M.A., 1988. Evidence for a new geomagnetic reversal from lava flows in Idaho: discussion of short polarity reversals in the Brunhes and late Matuyama polarity chrons. J. Geophys. Res. 93, 11667–11680.

Channell, J.E.T., 2006. Late Brunhes polarity excursions (Mono Lake, Laschamp Iceland Basin and Pringle Falls) recorded at ODP Site 919 (Irminger Basin). Earth Planet. Sci. Lett. 244, 378–393.

Channell, J.E.T., 1999. Geomagnetic paleointensity and directional secular variation at Ocean Drilling Program (ODP) Site 984 (Bjorn Drift) since 500 ka: comparisons with ODP Site 983 (Gardar Drift). J. Geophys. Res. 104, 22937–22951.

Channell, J.E.T., Curtis, J.H., Flower, B.P., 2004. The Matuyama–Brunhes boundary interval (500–900 ka) in North Atlantic drift sediments. Geophys. J. Int. 158, 489–505.

Channell, J.E.T., Raymo, M.E., 2003. Paleomagnetic record at ODP Site 980 (Feni Drift, Rockall) for the past 1.2 Myrs. Geochem. Geophys. Geosyst. (G^3) 4, 1033, doi:10.1029/2002GC000440.

Channell, J.E.T., Stoner, J.S., Hoddell, D.A., Charles, C., 2000. Geomagnetic paleointensity for the last 100 kyr from the subantarctic South Atlantic: a tool for interhemispheric correlation. Earth Planet. Sci. Lett. 175, 145–160.

Coe, R.S., 1967. Paleo-intensities of the Earth's magnetic field determiend from Tertiary and Quaternary rocks. J. Geophys. Res. 72, 3247–3262.

Coe, R.S., Singer, B.S., Pringle, M.S., Zhao, X., 2004. Matuyama–Brunhes reversal and Kamikatsura Event on Maui: paleomagnetic directions $^{40}Ar/^{39}Ar$ ages and implications. Earth Planet. Sci. Lett. 222, 667–684.

Constable, C., 2007. Nondipole field. In: Gubbins, D., Herrero-Bervera, E. (Eds.), Encyclopedia of Geomagnetism and Paleomagnetism. Springer, pp. 701–704.

Fuhrmann, U., Lippolt, H.J., 1987. Excess argon and dating of Quaternary Eifel volcanism. III. Alkalibasaltic rocks of the Central West Eifel FR Germany. Neues Jb. Geol. Paläont. Mh. H4, 213–236.

Glen, J.M., Coe, R.S., Liddicoat, J.C., 1999. A detailed record of paleomagnetic field change from the Searles Lake California 2. The Gauss/Matuyama polarity reversal. J. Geophys. Res. 104, 12883–12894.

Glen, J.M., Coe, R.S., Liddicoat, J.C., 1994. Persistent features of polarity transition records from western North America. Geophys. Res. Lett. 21, 165–1168.

Gubbins, D., 1999. The distinction between geomagnetic excursions and reversals. Geophys. J. Int. 137, F1–F3.

Guillou, H., Singer, B.S., Laj, C., Kissel, C., Scaillet, S., Jicha, B., 2004. On the age of the Laschamp geomagnetic event. Earth Planet. Sci. Lett. 227, 331–343.

Guyodo, Y., Valet, J.-P., 1999. Global changes in intensity of the Earth's magnetic field during the past 800 kyr. Nature 399, 249–252.

Hillhouse, J., Cox, A., 1976. Brunhes–Matuyama polarity transition. Earth Planet. Sci. Lett. 29, 51–64.

Hofffman, K.A., 1992. Dipolar reversal states of the geomagnetic field and core–mantle dynamics. Nature 359, 789–794.

Hoffman, K.A., Singer, B.S., 2004. Regionally recurrent paleomagnetic transitional fields and mantle processes. In: Channell, J.E.T., et al. (Eds.), Timescales of the Paleomagnetic Field, 145. Amer. Geophys. Union, Geophys. Monogr. Ser., pp. 233–243.

Jackson, A., Jonkers, A.R.T., Walker, M.R., 2000. Four centuries of geomagnetic secular variation from historical records. Philos. Trans. R. Soc. Lond. Ser. A 358, 957–990.

Keyser, M., Ritter, J.R.R., Jordan, M., 2002. 3D shear-wave velocity structure of the Eifel plume Germany. Earth Planet. Sci. Lett. 203, 59–82.

Knudsen, M.F., Abrahmson, N., Riisiger, P., 2003. Paleomagnetic evidence from Cape Verde Islands basalts for fully reversed excursions in the Brunhes Chron. Earth Planet. Sci. Lett. 206, 199–214.

Laj, C., Mazaud, A., Weeks, R., Fuller, M.D., Herrero-Bervera, E., 1991. Geomagnetic reversal paths. Nature 351, 447.

Laj, C., Channell, J.E.T., 2007. Geomagnetic excursions. In: Kono, M. (Ed.), Treatise in Geophysics: vol. 5, Geomagnetism, Encyclopedia of Geophysics, pp. 373–416 (Chapter 10).

Laj, C., Kissel, C., Roberts, A.P., 2006. Geomagnetic field behavior during the Iceland Basin and Laschamp geomagnetic excursions: a simple transitional field geometry? Geochem. Geophys. Geosyst. 7, Q03004, doi:10.1029/2005GC001122.

Laj, C., Kissel, C., Beer, J., 2004. High resolution global paleointensity stack since 75 kyr (GLOPIS-75) calibrated to absolute values. In: Channell, J.E.T., Kent, D.V., Lowrie, W., Meert, J.G. (Eds.), Timescales of the Paleomagnetic Field, 145. Amer. Geophys. Union, Geophys. Mono., pp. 255–265.

Langereis, C.G., Dekkers, M.J., de Lange, G.J., Paterne, M., van Santvoort, P.J.M., 1997. Magnetostratigraphy and astronomical calibration of the last 1.1 Myr from an

eastern Mediterranean piston core and dating of short events in the Brunhes. Geophys. J. Int. 129, 75–94.
Lanphere, M.A., 2000. Comparison of conventional K–Ar and $^{40}Ar/^{39}Ar$ dating of young mafic rocks. Quat. Res. 53, 294–301.
Ludwig, K.R., 2003. Using Isoplot/Ex, Version 2.01: A Geochronological Toolkit for Microsoft Excel. Berkeley Geochronology Center Special Publication, Berkeley Geochronology Center, Berkeley, CA, 47 pp.
Lund, S.P., Acton, G., Clement, B., Hastedt, M., Okada, M., Williams, T., ODP Leg 172 Scientific Party, 1998. Geomagnetic field excursions ocurred often during the last million years. Trans. Am. Geophys. Union (EOS) 79 (14), 178–179.
Lund, S.P., Acton, G.D., Clement, B., Okada, M., Williams, T., 2001a. Brunhes Chron magnetic field excursions recovered from Leg 172 sediments. In: Keigwin, L.D., Rio, D., Acton, G.D., Arnold, E. (Eds.), Proc. ODP Sci. Res. S 172, 1–18 (Online).
Lund, S.P., Acton, G.D., Clement, B., Okada, M., Williams, T., 2001b. Paleomagnetic records of Stage 3 excursions Leg 172. In: Keigwin, L.D., Rio, D., Acton, G.D., Arnold, E. (Eds.), Proc. ODP Sci. Res. S 172, 1–20 (Online).
Lund, S.P., Stoner, J.S., Channell, J.E.T., Acton, G., 2006. A summary of Brunhes paleomagnetic field variability recorded in ODP Cores. Phys. Earth Planet. Inter. 156, 194–204.
Merrill, R.T., McFadden, P.L., 2005. The use of field excursions in stratigraphy. Quat. Res. 63, 232–237.
Mertes, H., Schmincke, H.U., 1983. Age distribution of volcanoes in the West Eifel. Neues Jb. Geol. Paläont. Abh. 166, 260–293.
Olsen, N., 2002. A model of the geomagnetic field and its secular variation for epoch 2000. Geophys. J. Int. 149, 454–462.
Renne, P.R., Swisher, C.C., Deino, A.L., Karner, D.B., Owens, T.L., DePaolo, D.J., 1998. Intercalibration of standards, absolute ages and uncertainties in $^{40}Ar/^{39}Ar$ dating. Chem. Geol. 145, 117–152.
Schmincke, H.U., Lorenz, V., Seck, H., 1983. The Quaternary Eifel volcanic fields. In: Fuchs, K., von, G.K., Mälzer, H., Murawski, H., Semmel, A. (Eds.), Plateau Uplift. Springer-Verlag, Berlin, pp. 139–151.
Schnepp, E., 1992. Paleointensity in the Quaternary West Eifel volcanic field, Germany: preliminary results. Phys. Earth Planet. Int. 70, 231–236.
Schnepp, E., 1994. Determination of paleointensities from the Quaternary West Eifel volcanic field, Germany. Geophys. J. Int. 116, 688–714.
Schnepp, E., Hradetzky, H., 1994. Combined paleointensity and $^{40}Ar/^{39}Ar$ age spectrum data from volcanic rocks of the West Eifel field (Germany): evidence for an early Brunhes geomagnetic excursion. J. Geophys. Res. 99, 9061–9076.
Shaw, C.S.J., 2004. The temporal evolution of three magmatic systems in the West Eifel volcanic field Germany. J. Volcanol. Geotherm. Res. 131, 213–240.
Singer, B.S., 2007. Polarity transitions: radioisotopic dating. In: Gubbins, D., Herrero-Bervera, E. (Eds.), Encyclopedia of Geomagnetism and Paleomagnetism. Springer, pp. 834–839.
Singer, B.S., Hoffman, K.A., Chauvin, A., Coe, R.S., Pringle, M.S., 1999. Dating transitionally magnetized lavas of the late Matuyama Chron: toward a new $^{40}Ar/^{39}Ar$ timescale of reversals and events. J. Geophys. Res. 104, 679–693.
Singer, B.S., Relle, M.K., Hoffman, K.A., Battle, A., Laj, C., Guillou, H., Carracedo, J.C., 2002. $^{40}Ar/^{39}Ar$ ages from transitionally magnetized lavas on La Palma, Canary Islands, and the geomagnetic instability timescale. J. Geophys. Res. 107, 2307, doi:10.1029/2001JB001613.
Singer, B.S., Brown, L.L., Rabassa, J.O., Guillou, H., 2004a. $^{40}Ar/^{39}Ar$ chronology of late Pliocene and Early Pleistocene geomagnetic and glacial events in southern Argentina. In: Channell, J.E.T., et al. (Eds.), Timescales of the Paleomagnetic Field, 145. AGU Geophys. Monogr. Ser., pp. 175–190.
Singer, B.S., Ackert Jr., R.P., Guillou, H., 2004b. $^{40}Ar/^{39}Ar$ and K–Ar chronology of Pleistocene glaciations in Patagonia. Geol. Soc. Am. Bull. 116, 434–450.
Singer, B.S., Jicha, B.R., Kirby, B.T., Geissman, J.W., Herrero-Bervera, E., 2008. $^{40}Ar/^{39}Ar$ dating links Albuquerque Volcanoes to the Pringle Falls excursion and the Geomagnetic Instability Time Scale. Earth Planet. Sci. Lett. 267, 584–595, doi:10.1016/j.epsl.2007.12.009. -0019.
Singer, B.S., Hoffman, K.A., Coe, R.S., Brown, L.L., Jicha, B.R., Pringle, M.S., Chauvin, A., 2005. Structural and temporal requirements for geomagnetic field reversal deduced from lava flows. Nature 434, 633–636.
Steiger, R.H., Jäger, E., 1977. Subcomission on geochronology: convention on the use of decay constants in geo- and cosmochronology. Earth Planet. Sci. Lett. 5, 320–324.
Stoner, J.S., Laj, C., Channell, J.E.T., Kissell, C., 2002. South Atlantic and North Atlantic paleointensity stacks (0–80 ka): implications for inter-hemispheric correlation. Quat. Sci. Rev. 21, 1141–1151.
Thellier, E., Thellier, O., 1959. Sur l'intensité du champ magnetique terrestre dans le passé historique et géologique. Ann. Geophys. 15, 285–376.
Zöller, L., 1989. Das Alter des Mosenberg Vulkans in der Vulkaneifel. Die Eifel 84, 415–418.